by ±14° with an automated goniometer to reverse the soft-layer magnetization, using the in-plane magnetic field of ±200 Oe (the hard CoPtCr film had been saturated by applying a 10-kOe in-plane field). Lorentz images were recorded at the sample tilt corresponding to −200 Oe when the soft FM layer was saturated and the remaining image contrast was due to residual magnetization ripple in the CoPtCr hard layer. All Lorentz images were recorded under identical conditions and were carefully aligned so that changes in contrast could be related to microstructural and micromagnetic features. Using image subtraction, contrast changes could be monitored, allowing the nucleation and growth of magnetic domains within the hard layer to be identified.

13. Y. Zheng and J.-G. Zhu, *J. Appl. Phys.* **81**, 5470 (1997).
14. A. Hubert, *Phys. Stat. Sol.* **38**, 699 (1970).

15. Partly supported by funding from the Advanced MRAM Project of the Defense Advanced Research Projects Agency. We acknowledge the use of facilities at the Center for High Resolution Electron Microscopy at Arizona State University. M.R.S. and S.S.P.P. thank P. Trouilloud of the IBM T.J. Watson Research Center for discussions that contributed substantially to this work, and we thank J. Speidell for supplying silicon nitride membranes.

19 July 1999; accepted 5 October 1999

Detection of Nonthermal Melting by Ultrafast X-ray Diffraction

C. W. Siders,[1]* A. Cavalleri,[1] K. Sokolowski-Tinten,[4] Cs. Tóth,[2] T. Guo,[1]† M. Kammler,[5] M. Horn von Hoegen,[6]‡ K. R. Wilson,[1] D. von der Linde,[4] C. P. J. Barty[3]

Using ultrafast, time-resolved, 1.54 angstrom x-ray diffraction, thermal and ultrafast nonthermal melting of germanium, involving passage through nonequilibrium extreme states of matter, was observed. Such ultrafast, optical-pump, x-ray diffraction probe measurements provide a way to study many other transient processes in physics, chemistry, and biology, including direct observation of the atomic motion by which many solid-state processes and chemical and biochemical reactions take place.

Many fundamental processes in nature, such as chemical and biochemical reactions and phase transitions, involve changes in the structure of matter: rearrangement of the constituent atoms and molecules. Such changes usually occur transiently on time scales that are comparable with the natural oscillation periods of atoms and molecules; that is, femtoseconds to picoseconds. Ultrashort-pulse visible lasers with such pulse widths have been used for more than two decades to optically pump and dynamically probe a wide array of atomic, molecular, solid-state, and plasma systems, including extreme states of matter normally found only in stellar or planetary interiors and experimentally accessible only by the rapid heating and inertial confinement made possible with ultrashort-pulse irradiation (*1*, *2*). In these experiments, however, the visible light used to probe the ensuing dynamics inherently cannot resolve atomic-scale features, and it interacts predominately with valence and free electrons and not with the deeper lying core electrons and nuclei that most directly indicate structure. Hard x-ray radiation, with wavelengths comparable with interatomic distances, is well suited to measure structure and atomic rearrangement and can measure structural dynamics in the interior of samples that are not transparent to ordinary light. Recently, subpicosecond sources of hard x-rays have been developed (*3*–*5*), making possible new classes of experiments in physics, chemistry, and biology (*4*, *6*–*9*). Visible-pump, x-ray diffraction probe experiments that measure the generation and propagation of coherent acoustic pulses in bulk gallium arsenide (GaAs) crystals have been reported (*7*). In those experiments, milli-angstrom changes in lattice spacing were measured with picosecond temporal resolution. Here we report on the observation, using time-resolved x-ray diffraction, of ultrafast nonthermal melting of short-pulse–irradiated germanium (Ge) (*10*).

In general, if a solid is heated to or above the melting temperature, nucleation of the liquid phase occurs around crystal defects or inclusions, usually at the surface itself, and the rate of phase change depends on the degree of superheating of the solid (*11*). In the case of laser irradiation of an absorbing crystalline semiconductor, incident optical energy is initially coupled to the carriers, which undergo band-to-band transitions. Intraband relaxation and nonradiative recombination cause delayed heating of the lattice (*12*), which exceeds the melting temperature within several picoseconds. After nucleation of the liquid phase at the surface, a thin liquid layer grows into the bulk of the material at a velocity depending on the degree of superheating of the interface but limited by the speed of sound. Typically, a layer a few tens of nanometers thick will melt in a few hundred picoseconds (*13*). This effect has been observed for irradiation with pulses longer than several picoseconds (*14*) and for near-threshold femtosecond pulses. In contrast, optical experiments using fluences twice the melting threshold or greater (*15*–*20*) exhibit a significantly faster, subpicosecond change of the linear optical properties at the surface, with reflectivities reaching, in a few hundred femtoseconds, values equal to that of the conventional liquid phase (*18*, *19*). In other experiments, a reduction in the second-harmonic-in-reflection signal, suggesting a subpicosecond loss of crystalline order at the very surface, was also seen (*15*, *16*, *18*). These observations indirectly indicate that an ultrafast solid-to-liquid phase transition occurs at the surface of the semiconductor on a time scale faster than carrier-lattice equilibration times. In order to directly observe the nonthermal loss of crystalline order both at the surface and in the bulk of the semiconductor lattice, we performed time-resolved, optical-pump, ultrafast x-ray diffraction probe experiments on laser-irradiated Ge.

Three samples, nominally 160 nm thick, were used, consisting of single-crystal Ge films grown by means of a novel surfactant-mediated growth technique (*21*) over large areas (7.6 cm in diameter) of single-crystal silicon substrates. These large-area layered samples allowed us to acquire data (*22*) using the same standards routinely used in ultrafast optical studies of nonreversible dynamics of solids: First, because the film thickness was smaller than both the optical and x-ray penetration lengths, the entire x-ray–probed depth was optically pumped; second, the large area permitted shot-by-shot sample translation at the 20-Hz laser repetition rate, thereby illuminating a fresh area of the sample on every shot.

Diffraction images were measured at different pump-probe time delays (Fig. 1). Because the diffracted x-rays emanated from a point source, the horizontal axis on the detector represents various diffraction angles, whereas the vertical axis gives the scattering position on the sample. The diffraction image taken at negative time delays (Fig. 1A) is identical to the unpumped case. The $K_{\alpha 1}$ and $K_{\alpha 2}$ spin-orbit-split lines of Cu are clearly

[1]Department of Chemistry and Biochemistry, [2]Institute for Nonlinear Science, [3]Department of Applied Mechanical/Engineering Sciences, University of California, San Diego, La Jolla, CA 92093–0339, USA. [4]Institut für Laser- und Plasmaphysik, Universität Essen, D-45117 Essen, Germany. [5]Institut für Halbleitertechnologie, [6]Institut für Festkörperphysik, Universität Hannover, D-30167 Hannover, Germany.

*To whom correspondence should be addressed. E-mail: csiders@ucsd.edu.
†Present address: Department of Chemistry, University of California, Davis, Davis, CA 95616, USA.
‡Present address: Institut für Laser- und Plasmaphysik, Universität Essen, D-45117 Essen, Germany.

resolved with bulk Ge, approximately 100 arcsec apart, with linewidth-limited resolution. With the 160-nm films, we measured the linewidth-convolved rocking curve of the thin film and did not resolve the individual $K_{\alpha 1}$ and $K_{\alpha 2}$ lines. To reach a sufficiently high signal-to-noise ratio, photon counting for 200 laser shots was required. Given this, our pumped area, and the total area of our samples, we were limited to measuring only nine delay points and could not exhaustively acquire data on the subpicosecond time scale. We set the zero time delay with ±1-ps accuracy by measuring strain generation in a reversible configuration (*7*) at approximately one-10th the melting fluence and determining the latest time delay at which no appreciable strain was discernible. The diffraction image taken at a delay of +6.7 ps (Fig. 1B) shows an area of reduced diffraction, indicating disordering in the center of the pumped spot. At later time delays (Fig. 1C), the area widened over which the reduced diffraction (and hence disordering) took place. A slower disordering process was observed in the outer areas of the pumped spot, where the fluence was closer to the melting threshold. The image taken at a delay of +107 ps (Fig. 1D) shows a broad disordered area, as well as a shift of the reduced-intensity Bragg line, in the pumped region, toward lower diffraction angles, which suggests that the solid Ge layer beneath the melt was strained by thermal expansion (*7*, *23*). Finally, a nonrastered diffraction image (Fig. 1E) taken several seconds after irradiation on a vertical sequence of single-shot damage spots shows nearly complete recovery of the diffraction signal on a semi-infinite time scale.

In the plot of the integrated diffraction from the center (solid line) and edge (dashed line) of the pumped spot as a function of visible-pump x-ray probe delay (Fig. 2), the signal from the central region shows a sharp drop of ~20% within the first 7 ps, limited by the time delay between measurement steps, whereas the edge region retains the reflectivity of the unpumped crystal. A slower decay in integrated diffraction is seen in parallel in both regions on a longer time scale, and a drop in integrated diffraction of ~50% in the central region (~20% on the edge) is observed at a delay of 40 ps. At 107 ps delay, an increase in the diffraction signal is seen, possibly due to the fact that the expanded solid Ge has higher integrated diffraction efficiency than the unstrained crystal (*7*). At an infinite time delay, the diffraction signal recovers, for both regions, to ~90% of the initial value, showing that (111) crystalline order in the molten region is reestablished on the long time scale, with the incomplete return most likely due to partial ablation at the surface, where the fluence is high enough to generate a superheated liquid (*24*), or possibly to amorphous recrystallization of the molten Ge (*25*). This clearly rules out the possibility of a solid-gas or solid-plasma phase transition and demonstrates that we are observing a solid-to-liquid phase transition, followed by recrystallization.

Because the observed reduction in integrated diffraction efficiency in the central part of the pumped region is significantly greater than that expected from the Debye-Waller reduction for a highly superheated solid [for example, a 10% reduction for Ge(111) at 2000 K at 1.54 Å], we must conclude that a thin layer of the film loses crystalline order within a few picoseconds. Because the integrated x-ray reflectivity scales with the film thickness, approximately 20%, or 35 nm, of the 160-nm film must be disordered. Conventional thermal melting after rapid heating cannot account for this; even if we assume that the lattice instantaneously reaches the melting temperature, a supersonic melt front velocity of $\sim 10^4$ m/s would be required, exceeding the expected liquid-solid interface velocity by an order of magnitude (*15*, *26*) and exceeding the highest possible value by about a factor of 3. In addition, a delay of a few picoseconds for the lattice temperature to reach the melting temperature at the surface is expected because of screening of Auger recombination at the high carrier densities (6×10^{22} cm^{-3}, corresponding on average to more than one of the four valence electrons available from each Ge atom in the crystal) that are present immediately after absorption of our 0.5-J/cm^2, 100-fs, 800-nm laser pulse (*12*, *15*). Therefore, we must conclude that the Ge rapidly and homogeneously melts through a nonthermal disassembling process in the first few picoseconds after energy deposition. Indeed, an estimate of the carrier density distribution after absorption of the pump suggests that the excited carrier density exceeds the theoretically calculated lattice stability limit of 10^{22} cm^{-3} (*27*) over a depth of approximately 30 to 40 nm, which is in good agreement with our measured ~35-nm disordered depth.

At later times, one observes in the integrated diffraction signal a slower disordering process taking place at the same rate in the transverse edges of the illuminated region as well as deeper within the central pumped region. In these regions of the crystal, the absorbed energy is close to the melting threshold, and the disordering can evolve inhomogeneously along the thermal pathway described above (*20*). Similar behavior has been observed optically at the surface of GaAs under comparable laser absorption conditions (*20*) (2-eV radiation, 1.5-eV band-gap, and 250-nm penetration depth; conditions used here were as follows: 1.5-eV radiation, 0.8-eV direct band-gap, and 200-nm penetration depth). The slow drop at long times in the integrated diffraction efficiency (Fig. 2) suggests that thermal melting also occurs in the solid beneath the nonthermally molten surface layer. The observed reductions in both regions correspond to an average solid-liquid interface velocity of ~700 m/s at these later delay times, which is not unreasonable for thermal melting under highly superheated conditions (*26*).

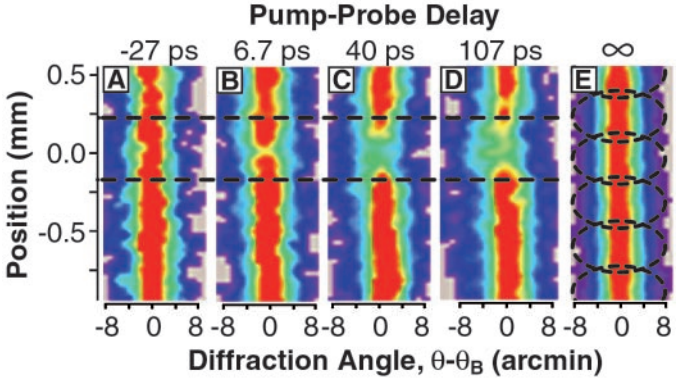

Fig. 1. Images obtained from a photon-counting x-ray area detector for five pump-probe time delays. The horizontal axis corresponds to the diffraction angle, shown relative to the Bragg angle for Ge. The vertical axis corresponds to the position on the semiconductor wafer. The optical pump photoexcites only a portion [indicated by dotted lines in (**A**) through (**D**)] of the entire x-ray–probed area. The image at infinite time delay (**E**), including six single-shot damage regions (indicated by dotted circles), was taken nonrastered and with the optical pump blocked during the exposure.

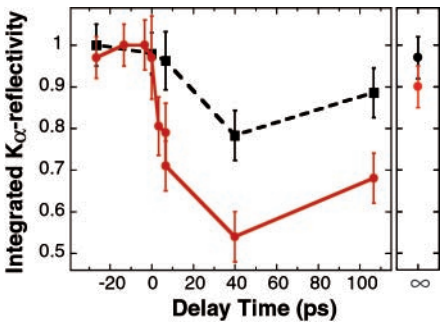

Fig. 2. Time-resolved K_α x-ray reflectivity from a 160-nm Ge(111) film, integrated over the central pumped region (solid red line) and over a region vertically displaced ~0.2 mm from the center (dashed black line).

These results demonstrate the ability of present-day ultrashort-laser–driven x-ray sources to study transiently generated extreme states of matter. Although further studies of important outstanding problems related to the structure of superheated solids and transient liquid phases (*1*, *2*) are natural extensions of this work, foreseeable improvements already in development in tabletop laser-driven plasma sources should expand the scope of ultrafast x-ray diffraction to the dynamic study of many other ultrafast processes in physics, chemistry, and biology, including the ultrafast atomic and molecular dynamics by which other solid-state processes and chemical and biochemical reactions take place.

References and Notes

1. N. Bloembergen, *Nature* **356**, 110 (1992); D. H. Reitze, H. Ahn, M. C. Downer, *Phys. Rev. B* **45**, 2677 (1992).
2. G. Galli, R. M. Martin, R. Car, M. Parrinello, *Science* **250**, 1547 (1990).
3. R. W. Schoenlein *et al.*, *Science* **274**, 236 (1996).
4. C. Rischel *et al.*, *Nature* **390**, 490 (1997).
5. M. M. Murnane, H. C. Kapteyn, M. D. Rosen, R. W. Falcone, *Science* **251**, 531 (1991).
6. J. Larsson *et al.*, *Appl. Phys. A* **66**, 587 (1998).
7. C. Rose-Petruck *et al.*, *Nature* **398**, 310 (1999).
8. A. H. Chin *et al.*, in *Ultrafast Phenomena XI*, T. Elsaesser, J. G. Fujimoto, D. A. Wiersma, W. Zinth, Eds. (Springer, Berlin, 1998), pp. 401–403.
9. A. Cavalleri *et al.*, Quantum Electronics and Laser Science Conference (QELS) '99, postdeadline session QPD8, Baltimore, MD (1999); A. Rousse, Conference on Lasers and Electro-optics (CLEO) '99, session JWC1, Baltimore, MD (1999); A. M. Lindenberg *et al.*, QELS '99, session QThJ4, Baltimore, MD (1999).
10. J. A. Van Vechten, R. Tsu, F. W. Saris, *Phys. Lett. A* **74A**, 422 (1979).
11. N. Fabricius, P. Hermes, D. von der Linde, A. Pospieszczyk, B. Stritzker, *Solid State Commun*. **58**, 239 (1986).
12. M. C. Downer and C. V. Shank, *Phys. Rev. Lett*. **56**, 761 (1986).
13. F. Spaepen and D. Turnbull, in *Laser Annealing of Semiconductors*, J. M. Poate and J. W. Mayer, Eds. (Academic Press, London, 1982), pp. 15–42.
14. R. F. Wood and C. W. White, *Pulsed Laser Processing of Semiconductors, Semiconductors and Semimetals* (Academic Press, Orlando, FL, 1984), vol. 23.
15. C. V. Shank, R. Yen, C. Hirlimann, *Phys. Rev. Lett*. **50**, 454 (1983); *Phys. Rev. Lett*. **51**, 900 (1983).
16. H. W. K. Tom, G. D. Aumiller, C. H. Brito-Cruz, *Phys. Rev. Lett*. **60**, 1438 (1988).
17. P. Saeta, J. K. Wang, Y. Siegal, N. Bloembergen, E. Mazur, *Phys. Rev. Lett*. **67**, 1023 (1991).
18. K. Sokolowski-Tinten, J. Bialkowski, D. von der Linde, *Phys. Rev. B* **51**, 14186 (1995).
19. H. Li, J. P. Callan, E. N. Glezer, E. Mazur, *Phys. Rev. Lett*. **80**, 185 (1998).
20. K. Sokolowski-Tinten, J. Bialkowski, M. Boing, A. Cavalleri, D. von der Linde, *Phys. Rev. B* **58**, R11805 (1998).
21. M. Horn-von Hoegen, M. Copel, J. C. Tsang, M. C. Reuter, R. M. Tromp, *Phys. Rev. B* **50**, 10811 (1994); M. Horn-von Hoegen, *Appl. Phys. A* **A59**, 503 (1994).
22. Our experimental setup, discussed previously in (*7*), consisted of a visible-pump x-ray probe apparatus, with which the 8-keV (1.54 Å) bursts of Cu-K_α line radiation were generated by focusing 80-mJ, 30-fs pulses from a multiterawatt laser (*28*) at relativistic intensities onto a moving copper wire. X-ray pulses emitted from the plasma point source were diffracted by a photoexcited (111)-Ge crystal in a symmetric Bragg configuration and were recorded with a photon-counting area detector. The optical pump pulse, split off from the x-ray–generating laser pulse, was independently adjustable in both energy and pulsewidth. Focused onto the sample with a cylindrical lens, the pump pulse illuminated a ~0.4 mm by 2 mm region of the crystal that was sufficiently larger in the angular (that is, horizontal) direction than the area probed by the x-rays. Using a silicon wafer target, the pump fluence was first empirically set to the melting fluence of silicon, as evidenced by post-irradiation examination (*29*), and then increased to 0.5 J/cm^2, which is more than twice the known melting threshold for Ge. To avoid plasma formation in air or at the surface of the sample, the pump-pulse duration was increased to 100 fs, where no effects of plasma formation were observed.
23. B. C. Larson, C. W. White, T. S. Noggle, D. Mills, *Phys. Rev. Lett*. **48**, 337 (1982).
24. K. Sokolowski-Tinten *et al.*, *Phys. Rev. Lett*. **81**, 224 (1998).
25. Postmortem examination with interference microscopy did indicate crater formation, with an estimated upper limit of a crater depth of 15 nm. As expected from optical measurements (*24*), the crater diameter was significantly smaller than the transiently disordered area. Amorphous rings (*29*), which were observed with bulk silicon samples used to set the incident fluence, were not visible on the Ge films.
26. D. von der Linde, in *Resonances*, M. D. Levenson, E. Mazur, P. S. Pershan, Y. R. Shen, Eds. (World Scientific, Singapore, 1990).
27. P. Stampfli and K. H. Bennemann, *Phys. Rev. B* **49**, 7299 (1994); *Phys. Rev. B* **46**, 10686 (1992); *Phys. Rev. B* **42**, 7163 (1990).
28. C. P. J. Barty *et al.*, *Opt. Lett*. **21**, 668 (1996).
29. J. M. Liu, *Opt. Lett*. **7**, 196 (1982).

30. K.S.T. gratefully acknowledges financial support by the Deutsche Forschungsgemeinschaft.

15 July 1999; accepted 23 September 1999

Cretaceous Sauropods from the Sahara and the Uneven Rate of Skeletal Evolution Among Dinosaurs

Paul C. Sereno,[1]* Allison L. Beck,[1] Didier B. Dutheil,[2] Hans C. E. Larsson,[1] Gabrielle H. Lyon,[3] Bourahima Moussa,[4] Rudyard W. Sadleir,[5] Christian A. Sidor,[1] David J. Varricchio,[6] Gregory P. Wilson,[7] Jeffrey A. Wilson[8]

Lower Cretaceous fossils from central Niger document the succession of sauropod dinosaurs on Africa as it drifted into geographic isolation. A new broad-toothed genus of Neocomian age (~135 million years ago) shows few of the specializations of other Cretaceous sauropods. A new small-bodied sauropod of Aptian-Albian age (~110 million years ago), in contrast, reveals the highly modified cranial form of rebbachisaurid diplodocoids. Rates of skeletal change in sauropods and other major groups of dinosaurs are estimated quantitatively and shown to be highly variable.

Breakup of the supercontinent Pangaea resulted in the differentiation of dinosaurian faunas that had been relatively uniform until the close of the Jurassic (*1*). Recent fossil discoveries on southern continents highlight the complexity of Cretaceous dinosaurian faunas (*2*–*4*). We report here on two new sauropod dinosaurs from central Niger that document the succession of these gigantic herbivores on northern Africa during the Early Cretaceous.

The fossils were discovered at several localities in the Neocomian [~140 to 130 million years ago (Ma)] Tiourarén Formation and in Aptian-Albian (~115 to 105 Ma) horizons of the Tegama Group in the Gadoufaoua region (Fig. 1).

The sauropod from the Tiourarén Formation, *Jobaria tiguidensis* gen. nov. sp. nov. (*5*), is the most abundant terrestrial vertebrate in the formation; no remains of any other large-bodied herbivore were recovered. The formation consists predominantly of clay-rich overbank deposits, which in one locality have entombed several partial skeletons of different sizes (*6*) (Fako; Fig. 1A, locality 3). Associated dinosaurs include the theropod *Afrovenator* (*3*) and two smaller bodied predators of uncertain affinities.

The skull (Fig. 2, A and B) is proportionately smaller and lighter in construction than that in *Camarasaurus*. The total length of an

[1]Department of Organismal Biology and Anatomy, University of Chicago, 1027 East 57 Street, Chicago, IL 60637, USA. [2]Laboratoire de Paléontologie–EPHE–Muséum National d'Histoire Naturelle, 8 rue du Buffon, 75005 Paris, France. [3]Project Exploration, 5521 South Blackstone Avenue, Chicago, IL 60637, USA. [4]Centre des Sciences de la Terre, Centre National de Recherche Scientifique, 6 Boulevard Gabriel, 2100 Dijon, France. [5]Department of Earth and Environmental Sciences, University of Illinois at Chicago, 845 West Taylor Street, Chicago, IL 60607, USA. [6]Museum of the Rockies, Montana State University, Bozeman, MT 59717, USA. [7]University of California, Museum of Paleontology, 1101 Valley Life Sciences Building, Berkeley, CA 94720, USA. [8]Museum of Paleontology, University of Michigan, 1109 Geddes Road, Ann Arbor, MI 48109, USA.

*To whom correspondence should be addressed. Successive authors are listed alphabetically.